Hindawi Publishing Corporation
Journal of Nanomaterials
Volume 2015, Article ID 563728, 7 pages
http://dx.doi.org/10.1155/2015/563728

Research Article

Easy Formation of Nanodisk-Dendritic ZnO Film via Controlled Electrodeposition Process

Nur Azimah Abd Samad, Chin Wei Lai, and Sharifah Bee Abd Hamid

Nanotechnology & Catalysis Research Centre (NANOCAT), 3rd Floor, Block A, Institute of Postgraduate Studies (IPS), University of Malaya, 50603 Kuala Lumpur, Malaysia

Correspondence should be addressed to Chin Wei Lai; cwlai@um.edu.my

Received 29 June 2015; Revised 24 September 2015; Accepted 29 September 2015

Academic Editor: Thomas Fix

A facile electrodeposition synthesis was introduced to prepare the nanodisk-dendritic ZnO film using a mixture solution of zinc chloride ($ZnCl_2$) with potassium chloride (KCl) that acted as a directing agent. This study aims to determine the best photoelectrochemical response for solar-induced water splitting. Based on our results obtained, it was found that an average diagonal of nanodisk was approximately 1.70 μm with the thickness of ≈150 nm that was successfully grown on the surface of substrate. The photocatalytic and photoelectrochemical responses of the resultant wurtzite type based-nanodisk-dendrite ZnO film as compared to the as-prepared ZnO film were monitored and evaluated. A photocurrent density of 19.87 mA/cm^2 under ultraviolet rays and 14.05 mA/cm^2 under visible light (500 nm) was recorded for the newly developed nanodisk-dendritic ZnO thin film. It was believed that nanodisk-dendritic ZnO film can harvest more incident photons from the illumination to generate more photoinduced charge carriers to trigger the photocatalytic and photoelectrochemical reactions. Moreover, strong light scattering effects and high specific surface area of 2D nanostructures aid in the incident light absorption from any direction.

1. Introduction

Behind the rapid development of social, economic, and technology, energy becomes a crucial issue around the globe. A global warming devastation occurs from time to time and is becoming severe in the 21st century. Abrupt climate change happens around the world. Intergovernmental Panel on Climate Change (IPCC) is the responsible body to control the global temperature variation; it had announced that the global temperature absolutely increased with the estimation of 0.4 and 0.8°C for the past century and this phenomenon was the 10 warmest years over the last 15 years [1]. In the North Atlantic, the atmospheric circulation above Greenland also changed abruptly due to the global warming [2, 3]. Global warming phenomenon occurred as a result of greenhouse effect which led to the increasing in atmospheric temperature [3]. Increases in concentration of greenhouse gases such as nitrous oxide (N_2O), methane (CH_4), and carbon dioxide (CO_2) were the main causes of the drought in the areas from East Africa coastal area to the Arabian Sea, South Asia, East Asia, and South China. In the case of water (sea/river) level rising during the 21st century, global warming resulted in the melting of remaining ice masses. IPCC forecasts global mean sea levels (GMSLs) are likely to increase with the variation of 4-5 mm/year by 2050, 0.5–0.9 m by 2100, thus the losses of up to 30% of coastal wetlands [4]. Two major net heat sources had documented (1) net heating generated by human activities and (2) geothermal heat flow. In addition, the exploitation of nuclear energy and nonrenewable energy thus produces an additional heat in the world [5]. These driving forces lead the researchers to reduce the greenhouse effect and environmental protection with presenting creative ideas. In this paper, we are focusing on the alternative energy, hydrogen gas production. Today's hydrogen production is produced from fossil fuels, methane, and coal gasification [6]. The production of hydrogen gas determines the environmental impact and energy efficiency. Light-induced water splitting system is attractive to be studied. Thus, the photocatalysed degeneration of water with nanodisk-dendritic zinc oxide film was chosen to be the catalyst.

Zinc oxide is an n-type semiconductor, with direct wide band gap (3.37 eV) due to its electrons conductivity, and it has

Table 1: The different types of hexagonal ZnO disk based on preparation method.

Researcher	Preparation methods	Findings	References
Yin et al. (2014)	*Simple double-solvothermal method in the presence of glycine*	Complex superstructure was assembled by hexagonal disks; the thickness of the disk is about 300 nm	[25]
Zeng et al. (2009)	*Hydrothermal* method	Uniform single-crystalline ZnO nanodisks were well developed with 1.5 μm in diameter and 300 nm in thickness	[17]
Zhang et al. (2007)	*Electrodeposition* method, HBO_3 as an electrolyte with zinc foil as anode, voltage 180 V, and the system kept at 2°C	Zinc/ZnO core-shell hexagonal nanodisk dendrites were produced with diameter from about 100 nm to several hundred nanometers and thicknesses are about 20–40 nm.	[15]
Li et al. (2007)	*Electrochemical deposition* method	The shape of the ZnO dendritic structure is similar to the branch of a fern; ZnO dendritic structure is in the range of 6–10 μm and 200 nm of thickness	[26]
Xu et al. (2004)	*Vapour phase transport (VPT)* method	Zinc oxide nanodisk; 3 μm in diagonal and 300 nm in thickness	[21]

the wurtzite hexagonal crystal structure. The stoichiometric excess of zinc ions is believed to cause the electrons conductivity where the zinc ions live in interstitial locations in the crystal lattice [7]. The other property of ZnO is the high exciton binding energy (60 meV) in ZnO crystal which can produce efficient excitonic emission under room temperature ultraviolet (UV) luminescence [8–10]. Moreover, rectification, optical properties, and chemical properties of ZnO bring great interest to the research world [9–16]. Synthesis method will determine the crystal shape from acicular needles to plate shaped crystal. By all means, this is the uniqueness of zinc oxide which can be made to form into a variety of crystalline shapes [17]. Furthermore, nearly neutral (pH ~ 6) system applied to the formation of ZnO nanostructures supports the environmental protection [17]. According to Table 1, electrochemical deposition method is likely to produce nanodisk-dendritic ZnO and disk-shape morphology is less familiar in research. At the same time, it has unique properties and leads to potential applications such as water-splitting process [18], electrodes for dye sensitized solar cells [19], and nanosensors [20, 21]. Equally important, the low active surface area and fast recombination losses of photoinduced charge carriers remain as a great challenge for ZnO nanostructures. Therefore, in this paper, the formation of nanodisk-dendritic zinc oxide was studied. The ability of nanodisk-dendritic ZnO photoelectrode in current-voltage characteristics and methyl orange (MO) degradation also has been studied.

2. Experimental Section

2.1. Synthesis of Nanodisk-Dendritic ZnO. ZnO nanostructures films were produced by electrodeposition process of zinc (Zn) foil (thickness 0.25 mm, 99.9% trace metals basis, Sigma-Aldrich) in a bath with electrolytes composed of 50 mL of 0.5 mM zinc chloride ($ZnCl_2$) and 50 mL of 0.1 M potassium chloride (KCl) at 3.0 V at temperature of 80°C. From our literature studies, 3.0 V and 80°C were selected in our study because the polycrystalline structure of ZnO will start to evolve at this potential difference and temperature with obviously and randomly oriented grains. The as-prepared pH of electrolyte is about 5-6, which was measured using a pH meter Mettler Toledo InLab Expert Pro. The electrodeposition process was conducted with two-electrode configuration system, where platinum electrode served as anode and Zn foil served as cathode. This closed system was then connected to a DC power supply. After electrodeposition process, the nanodeposit has been rinsed thoroughly with acetone for analysis Emsure Acs, Iso, Reag. Ph Eur for analysis and dried at atmosphere. The deposited ZnO nanostructured film was then annealed at 600°C for 3 hours because the zinc peaks will be negligible and completely oxidised [15].

2.2. Characterizations of Nanodisk-Dendritic ZnO. The crystallinity and phase transition of the samples were analyzed by using Bruker D8 Advance equipped with EVA-Diffract Software (Germany) X-ray Diffraction (XRD) with Cu K_α radiation and wavelength λ = 1.5418 Å. Meanwhile, the surface and cross-sectional morphologies of the samples have been viewed by Field Emission Scanning Electron Microscopy (FESEM) Quanta FEG 450 and the elemental analysis of ZnO nanostructured film was determined with Hitachi Energy Dispersive X-Ray Spectroscopy (EDX) analysis.

To study the photocurrent density of the sample, a three-electrode PEC cell with nanodisk-dendritic ZnO film served as anode, a platinum rod as the cathode, and a saturated calomel electrode (SCE) as the reference electrode arranged in a quarts cell filled with 1 M sodium hydroxide (NaOH) containing 1 v% of ethylene glycol. A 150 W xenon lamp (Zolix

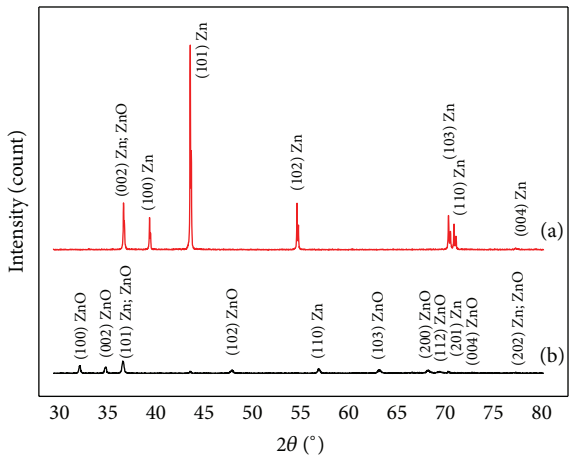

Figure 1: XRD pattern of (a) as-prepared ZnO and (b) annealed nanodisk-dendritic ZnO.

LSP-X150) was set to focus on the immersed portion of the photoelectrode to stimulate solar irradiation. The three electrodes were connected to the potentiostat (Metrohm Autolab PGSTAT204); the current-voltage value was measured. The photocurrent density has been measured by using Metrohm Autolab PGSTAT204, with linear sweep voltammetry potentiostatic procedure (−1 to 1 V potential applied). Photocatalytic degradation studies were implemented by dipping the nanodisk-dendritic ZnO thin film in 100 mL of 15 parts per million (ppm) of methyl orange (MO) solution in a quartz glass tube and placed in the photoreactor. The samples were photoilluminated at room temperature by using TUV 18 W UV-C Germicidal light. After leaving it in a reactor for 30 minutes in dark environment, 5 mL solution was withdrawn for every 1 hour from the quartz tubes to study the degradation of methyl orange (MO) after UV irradiation. A UV-Vis Spectrophotometer (UV-3101PC Shimadzu) was used to analyze the degradation percentage of MO solution.

3. Results and Discussion

3.1. Phase Transformation for Nanodisk-Dendritic ZnO. In this part of experiment, XRD analysis was used to investigate the crystallinity of the nanodisk-dendritic ZnO thin film and as-prepared ZnO thin film as presented in Figure 1. The XRD pattern of the as-prepared ZnO thin film exhibited major Zn phase, which points to the existence of amorphous nature (Figure 1(a)). The Bragg reflection of Zn phase was detected at 2θ values of 36.30°, 39.00°, 43.23°, 54.33°, 70.08°, 70.65°, and 77.02° in entire XRD patterns, corresponding to (002), (100), (101), (102), (013), (110), and (004) crystal planes, respectively. The presence of Zn phase was identified by ICDD file of 00-004-0831. Meanwhile, for nanodisk-dendritic ZnO thin film (Figure 1(b)), the result showed that the samples were in line with reference code ICDD 00-036-1451 which indicates the ZnO phase. The Bragg reflection of ZnO phase was detected at 2θ values of 31.75°, 34.51°, 36.31°, 47.60°, 62.29°, 66.41°, 67.94°, 70.02°, and 77.0° in entire XRD patterns, corresponding to (100), (002), (101), (102), (103), (200), (112), (004), and (202) crystal planes, respectively. It showed that the sample was crystallized and uniform lattice strain was obtained after calcination process. All peaks were shifted to the left as the ZnO crystals were well and denser after calcination process. In addition, the nanodisk-dendritic ZnO sample is matched with the chemical formula ZnO (referring to XRD test) and consists of hexagonal crystal system. Besides, it also matched the wurtzite type because a = 3.2498 Å, b = 3.2498 Å, and c = 5.2066 Å. The wurtzite type is important in semiconductor application as compared to other crystal structures of ZnO: zinc blende and rocksalt. The significance of wurtzite type ZnO was obtained from the ideal arrangement, by changing the c/a ratio or the u value. From experimental observation, c/a ratios are smaller than ideal ones. In addition, c/a ratio also showed the association of difference for two constituents' electronegativity. Consequently, components with the greatest difference show largest departure from the ideal c/a ratio [22–24].

Table 2: Average compositional ratio of nanodisk-dendritic ZnO and as-prepared ZnO using EDX spectroscopy analysis.

Element	Atomic percentage (%)	
	Nanodisk-dendritic ZnO	As-prepared ZnO
Zinc	42.59	84.32
Oxygen	57.41	15.68

3.2. Morphological Structure of Nanodisk-Dendritic ZnO. Substrate was shrill of nanodisk-dendritic ZnO (Figure 2(a)). The nanodisk-dendritic zinc oxides have a perfect hexagonal shape with diagonal of approximately 1.7 μm and thickness of approximately 150.4 nm. This result is in line with past researches at which nanodisk-dendritic ZnO exhibits unique characteristics and consists of overlapping nanodisks and self-tiered structure [15]. The stem and the leaflets were built of hexagonal nanodisks where they were self-arranged and self-assembled and became little leaves. The EDX spectroscopy analysis was performed and it showed average atomic percentage of 42.59% and 57.41% of zinc and oxygen, respectively, for nanodisk-dendritic ZnO and average atomic percentage of 84.32% and 15.68% of zinc and oxygen, respectively, for as-prepared ZnO (Table 2). In this study, two-step process took place under dynamic electrolyte for the formation of nanodisk-dendritic ZnO. The first step was the formation of zinc hydroxide ($Zn(OH)_2$), followed by formation of zinc oxide (ZnO). However, this process occurred at all time until the reaction stopped. In the first place, the process started with dissolution of zinc chloride, potassium chloride and water to potassium ion (K^+), zinc ion (Zn^{2+}), chloride ion (Cl^-), and hydroxide ion (OH^-) and formation of hydrogen gas (H_2) occurred in the electrolyte by electrochemical process with energy supplied from direct electric current that separated the electrolyte into ions [27, 28] (1). Second, for the formation of zinc hydroxide ($Zn(OH)_2$) (intermediate growth stage), the K^+ (as directing agent) attracted the OH^- to the cathode and produced increases in local pH, and saturation level changed at the cathode. When a supersaturation condition is reached, the nucleation of $Zn(OH)_2$ precipitation

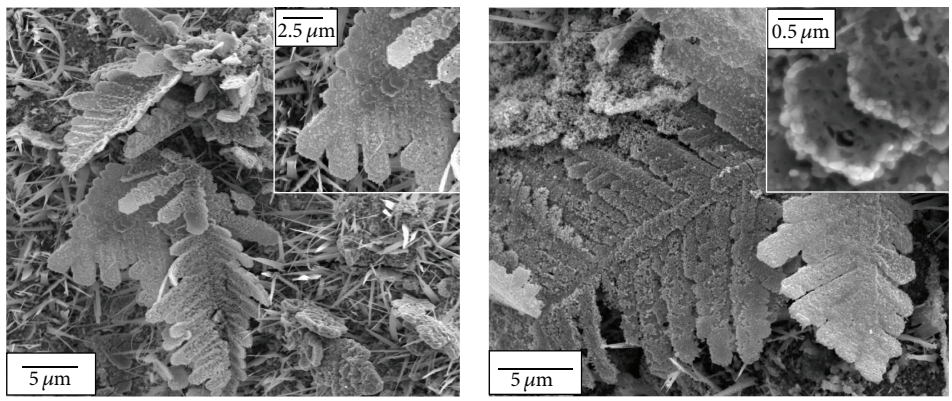

(a) (b)

Figure 2: FESEM image of (a) ×6k magnification of nanodisk-dendritic ZnO; (inset) ×20k magnification of stacked hexagonal-shape nanodisk ZnO and (b) ×10k magnification of nanodisk-dendritic ZnO; (inset) ×100k magnification hexagonal-shape nanodisk ZnO.

occurred on the substrate surface (cathode) (2). The formation of zinc oxide (ZnO) occurred by dehydration process of $Zn(OH)_2$ on the substrate (3). At the beginning of deposition process, the Zn^{2+} concentration at the substrate surface decreased when pH is increased leading to slowest growth rate towards (0001). Diffusion of Zn^{2+} from (0001) to the substrate surface leads to the unit growing at preferential growth of [1000] direction. When many nanodisks stacked together, it is important to realize that their arrangements on the substrate were on horizontal position (1000) which is in the x-axis direction and it is clearly seen in symmetry shape. The crystal growth velocity along various planes depended on the atomic packing density [15]. (Figure 2(a) inset and Figure 2(b) inset). Below are the equations related to the formation of ZnO:

Dissolution of $KCl + ZnCl_2 + H_2O$ is as follows:

$$\begin{aligned} KCl &\longrightarrow K^+(aq) + Cl^-(aq) \\ ZnCl_2 &\longrightarrow Zn^{2+}(aq) + 2Cl^-(aq) \\ 2H_2O &\longrightarrow H_2 \uparrow + 2OH^-(aq) \end{aligned} \quad (1)$$

Formation of zinc hydroxide ($Zn(OH)_2$), KOH, and KCl is as follows:

$$\begin{aligned} K^+(aq) + OH^-(aq) &\longrightarrow KOH \\ Zn^{2+}(aq) + 2OH^-(aq) &\longrightarrow Zn(OH)_2 \\ H_2 \uparrow + 2Cl^- &\longrightarrow 2HCl \end{aligned} \quad (2)$$

Formation of zinc oxide (ZnO) is as follows:

$$\begin{aligned} Zn(OH)_2 &\longrightarrow ZnO + H_2O \ (\text{dehydration process}) \\ HCl + KOH &\longrightarrow H_2O + KCl \end{aligned} \quad (3)$$

Past researches found the formation of dendrite shape due to the fast growth velocity of Zn ion in the electrolyte [29, 30]. Growth mechanism occurred in global diffusion and later oriented attachments were localized. Dislocation from the early crystal growth happened due to the high velocity of electrolyte (>350 rpm). Therefore, the second hexagonal nanodisk has grown slightly dislocated from the earlier crystal. Another key point is that nanodisk-dendritic tips were known to grow in the direction of maximum surface energy. The (1000) facet was out of sorts; therefore it contributed to highest effective surface energy [15, 31].

3.3. Photocatalytic Activity Evaluation. The photocatalytic activities of the nanodisk-dendritic ZnO and as-prepared ZnO were investigated using the MO degradation method under UV light radiation with the purpose to support the photocatalytic activity argument of nanodisk-dendritic ZnO. It was confirmed that nanodisk-dendritic ZnO exhibited good photocatalytic property when MO solution was degraded for approximately 80% after 6 hours under UV irradiation. Nanodisk-dendritic ZnO exhibited higher photocatalytic activity compared to as-prepared ZnO with MO concentration 18% after 6 hours (Figure 3(a)). Decomposition of MO solution can be explained by an oxidation process that took place on the surface of nanodisk-dendritic ZnO via photogenerated hole. In other words, an electron-hole pair existed in the absence of light intensity [32–34]. Under UV light illumination, energy produced was higher than nanodisk-dendritic ZnO band gap energy. Therefore, electrons at the conduction band and holes at the valence band were generated. Holes at the nanodisk-dendritic ZnO surfaces react with water to form highly reactive hydroxyl radicals ($OH^\bullet$), and at the same time oxygen acts as an electron acceptor by being a superoxide radical anion [35]. The superoxide radical anions from hydroxyl radicals have an excellent oxidation ability [36] which may degrade organic dye, and, in MO decomposition, it was degraded to carbon dioxide and water [31]. Nanodisk-dendritic ZnO showed high photocatalytic property due to its high surface area and active photoresponse (2D structure).

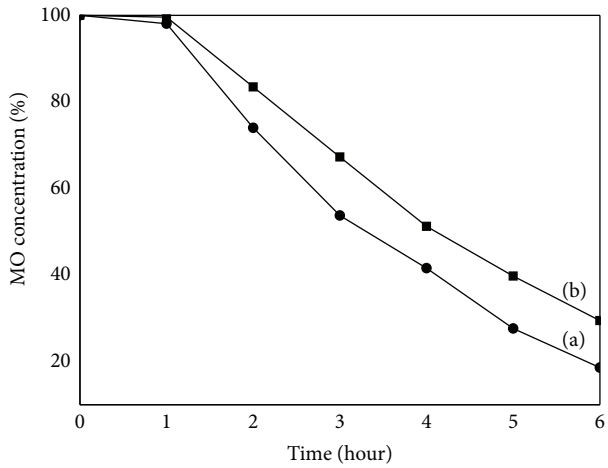

Figure 3: Photodegradation of MO solution by (a) nanodisk-dendritic ZnO and (b) as-prepared ZnO with increasing degradation time.

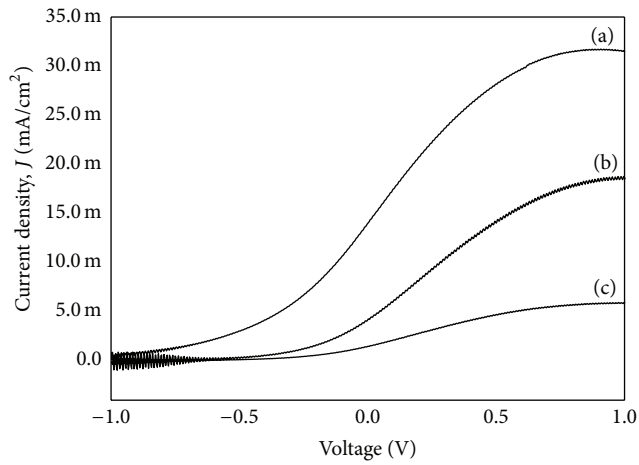

Figure 5: Current density-voltage characteristics for (a) nanodisk-dendritic ZnO, (b) as-prepared ZnO under visible light, and (c) nanodisk-dendritic ZnO without illumination.

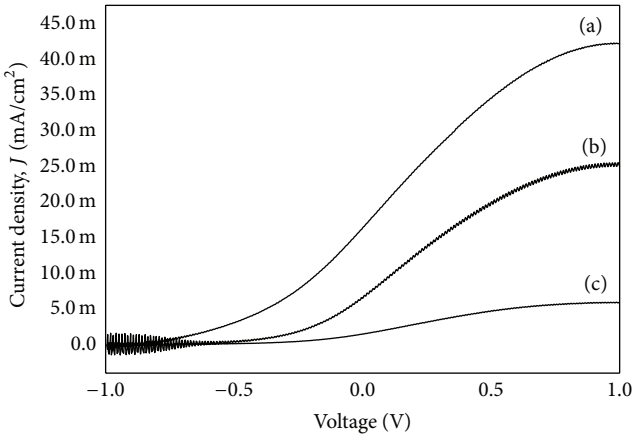

Figure 4: Current density-voltage characteristics for (a) nanodisk-dendritic ZnO and (b) as-prepared ZnO under ultraviolet ray and (c) nanodisk-dendritic ZnO without illumination.

3.4. Photoelectrochemical Response. A scanning potentiostat by mean to measure current (I) under an applied potential (V) could test the efficiency of nanodisk-dendritic ZnO photocatalytic activity. For water electrolysis application, the efficiencies of over 90% are at −1 to 1 V [37, 38]. From now on, in order to understand the efficiency nanodisk-dendritic ZnO thin films in water electrolysis, sample was evaluated and tested their I-V characteristics between −1 V and 1 V. Figure 4 was plotted to exhibit I-V characteristic curves for the (a) nanodisk-dendritic ZnO, (b) as-prepared ZnO under ultraviolet ray, and (c) nanodisk-dendritic ZnO without illumination. The significant photocurrent density j_p of an average value of 19.87 mA/cm^2 for nanodisk-dendritic ZnO under ultraviolet ray (Figure 4(a)) was obtained as compared to 6.45 mA/cm^2 for as-prepared ZnO under ultraviolet ray (Figure 4(b)) and 1.49 mA/cm^2 for nanodisk-dendritic ZnO without illumination (Figure 4(c)). The catalytic activity contribution can be observed from photocurrent density differences under ultraviolet ray illumination and without ultraviolet ray illumination. However, the current density j value decreased with the increasing of spectrum wavelength until visible light spectrum (390–700 nm) is reached. Under visible light, average j_p of 14.05 mA/cm^2 was observed for the nanodisk-dendritic ZnO (Figure 5(a)), which is relatively higher when compared to as-prepared ZnO under visible light: j_p 2.14 mA/cm^2 (Figure 5(b)) and nanodisk-dendritic ZnO without illumination: 1.49 mA/cm^2 (Figure 5(c)).

Based on the results of j-V characteristic curves (Figures 4 and 5), as-prepared-ZnO film showed poor result due to the existence of oxygen vacancies inside the ZnO bulk, which points to the increasing number of recombination centers. The recombination centers clearly contributed to the decreasing of photoinduced e^- mobility and back to the contact of Zn substrate because of series of resistance caused by increasing trap states. Besides, the amorphous phase comprises high concentration of other material defects such as impurities, dangling bonds, and microvoids, which similarly act as recombination center and result in a decrease of j_p [39]. Predominantly, as-prepared-ZnO film is basically unable to develop a regular depletion region [40]. It was found that the j_p of heat treated (600°C) nanodisk-dendritic ZnO sample was slightly increased to 19.87 mA/cm^2, which suggests that crystal structure of nanodisk-dendritic ZnO sample can improve the photocurrent generation effectively. In addition, the high specific surface area of nanodisk-dendritic architecture might have contributed to the strong light scattering effects and incident light absorption from any direction. In the electrolyte, the large active surface area established the photoinduced electrons and these electrons transferred to the substrate. By the use of external circuit, the photoinduced electron travels to counter electrode (platinum electrode) and enhances the photocatalytic activity and photoelectrochemical response significantly.

4. Conclusions

In this paper, nanodisk-dendritic ZnO with perfect hexagonal shape was fabricated by a simple one-step electrodeposition process with 600°C calcination temperature. From the characterization methods, it indicates that the sample is nanodisk-dendritic zinc oxide; with chemical formula, ZnO, and consists of hexagonal crystal system. It lies under tetragonal wurtzite type because a = 3.2498 Å, b = 3.2498 Å, and c = 5.2066 Å. The photocatalytic test (photocurrent density and methyl orange degradation) confirmed that nanodisk-dendritic zinc oxide has excellent photocatalytic activity. Prolonged electrodeposition time or increase of the $ZnCl_2$ concentration may increase the volume of nanodisk-dendritic ZnO and produce better photocatalytic activity.

Conflict of Interests

The authors declare that there is no conflict of interests regarding the publication of this paper.

Acknowledgments

The authors would like to thank University of Malaya for funding this research work under University of Malaya Research Grant (UMRG, RP022-2012D), Fundamental Research Grant Scheme (FRGS, FP055-2013B), and Postgraduate Research Fund Scheme (PPP, PG058-2014B). In addition, they would like to acknowledge Nippon Sheet Glass Foundation for Materials Science and Engineering (IF001-2015) for funding this research work.

References

[1] United States Environmental Protection Agency (EPA), *Global Warming*, United States Environmental Protection Agency (EPA), 2001.

[2] G. Bond, W. Showers, M. Cheseby et al., "A pervasive millennial-scale cycle in North Atlantic Holocene and glacial climates," *Science*, vol. 278, no. 5341, pp. 1257–1266, 1997.

[3] J.-B. Huang, S.-W. Wang, Y. Luo, Z.-C. Zhao, and X.-Y. Wen, "Debates on the causes of global warming," *Advances in Climate Change Research*, vol. 3, no. 1, pp. 38–44, 2012.

[4] R. J. Devoy, "Sea-level rise: causes, impacts, and scenarios for change," in *Coastal and Marine Hazards, Risks, and Disasters*, pp. 197–241, Elsevier, 2014.

[5] B. Nordell, "Thermal pollution causes global warming," *Global and Planetary Change*, vol. 38, no. 3-4, pp. 305–312, 2003.

[6] J. M. Ogden, "Prospects for building a hydrogen energy infrastructure," *Annual Review of Energy and the Environment*, vol. 24, no. 1, pp. 227–279, 1999.

[7] G. Vijayasarathi, "Alternate energy source using plants instead of photo-voltaic cell—an innovative solution for power crisis," *International Journal of Engineering Research & Technology*, vol. 1, no. 8, pp. 1–6, 2012.

[8] S. Roy and S. Basu, "Improved zinc oxide film for gas sensor applications," *Bulletin of Materials Science*, vol. 25, no. 6, pp. 513–515, 2002.

[9] Y. C. Kong, D. P. Yu, B. Zhang, W. Fang, and S. Q. Feng, "Ultraviolet-emitting ZnO nanowires synthesized by a physical vapor deposition approach," *Applied Physics Letters*, vol. 78, no. 4, pp. 407–409, 2001.

[10] Z. L. Wang, "Zinc oxide nanostructures: growth, properties and applications," *Journal of Physics: Condensed Matter*, vol. 16, no. 25, pp. R829–R858, 2004.

[11] S. Xu and Z. L. Wang, "One-dimensional ZnO nanostructures: solution growth and functional properties," *Nano Research*, vol. 4, no. 11, pp. 1013–1098, 2011.

[12] M. Abd-Ellah, N. Moghimi, L. Zhang et al., "Effect of electrolyte conductivity on controlled electrochemical synthesis of zinc oxide nanotubes and nanorods," *The Journal of Physical Chemistry C*, vol. 117, no. 13, pp. 6794–6799, 2013.

[13] C. J. Lee, T. J. Lee, S. C. Lyu, Y. Zhang, H. Ruh, and H. J. Lee, "Field emission from well-aligned zinc oxide nanowires grown at low temperature," *Applied Physics Letters*, vol. 81, no. 19, pp. 3648–3650, 2002.

[14] J. Zhang, M. Matsuoka, J. Sung Lee, and S. Chen, "Development of visible light-responsive photocatalysts," *International Journal of Photoenergy*, vol. 2012, Article ID 280297, 4 pages, 2012.

[15] X. Y. Zhang, J. Y. Dai, C. H. Lam et al., "Zinc/ZnO core-shell hexagonal nanodisk dendrites and their photoluminescence," *Acta Materialia*, vol. 55, no. 15, pp. 5039–5044, 2007.

[16] Y. Zhang, N. Wang, S. Gao et al., "A simple method to synthesize nanowires," *Chemistry of Materials*, vol. 14, no. 8, pp. 3564–3568, 2002.

[17] J. H. Zeng, B. B. Jin, and Y. F. Wang, "Facet enhanced photocatalytic effect with uniform single-crystalline zinc oxide nanodisks," *Chemical Physics Letters*, vol. 472, no. 1–3, pp. 90–95, 2009.

[18] S.-Y. Guo, S. Han, B. Chi, J. Pu, and J. Li, "Synthesis of shape-controlled mesoporous titanium phosphate nanocrystals: the hexagonal titanium phosphate with enhanced hydrogen generation from water splitting," *International Journal of Hydrogen Energy*, vol. 39, no. 6, pp. 2446–2453, 2014.

[19] Q. Zhang, C. S. Dandeneau, X. Zhou, and C. Cao, "ZnO nanostructures for dye-sensitized solar cells," *Advanced Materials*, vol. 21, no. 41, pp. 4087–4108, 2009.

[20] V. Germain, A. Brioude, D. Ingert, and M. P. Pileni, "Silver nanodisks: size selection via centrifugation and optical properties," *The Journal of Chemical Physics*, vol. 122, no. 12, Article ID 124707, 2005.

[21] C. X. Xu, X. W. Sun, Z. L. Dong, and M. B. Yu, "Zinc oxide nanodisk," *Applied Physics Letters*, vol. 85, no. 17, pp. 3878–3880, 2004.

[22] J. L. G. Fierro, *Metal Oxides: Chemistry and Applications*, CRC Press, 2010.

[23] E. H. Kisi and M. M. Elcombe, "u parameters for the wurtzite structure of ZnS and ZnO using powder neutron diffraction," *Acta Crystallographica—Section C: Crystal Structure Communications*, vol. 45, no. 12, pp. 1867–1870, 1989.

[24] M. O. Manasreh, *III-Nitride Semiconductors: Electrical, Structural and Defects Properties*, Elsevier, Amsterdam, The Netherlands, 2000.

[25] J. Yin, F. Gao, C. Wei, and Q. Lu, "Water amount dependence on morphologies and properties of ZnO nanostructures in double-solvent system," *Scientific Reports*, vol. 4, article 3736, 2014.

[26] G.-R. Li, X.-H. Lu, D.-L. Qu et al., "Electrochemical growth and control of ZnO dendritic structures," *Journal of Physical Chemistry C*, vol. 111, no. 18, pp. 6678–6683, 2007.

[27] B. Boddenberg, "Concepts in physical chemistry," *Zeitschrift für Physikalische Chemie*, vol. 195, part 1-2, pp. 287–289, 1996.

[28] J. M. Barthel, H. Krienke, and W. Kunz, *Physical Chemistry of Electrolyte Solutions: Modern Aspects*, vol. 5, Springer Science & Business Media, 1998.

[29] M. E. Perel'man, G. M. Rubinstein, and V. A. Tatartchenko, "Mechanisms of dendrites occurrence during crystallization: features of the ice crystals formation," *Physics Letters A*, vol. 372, no. 22, pp. 4100–4103, 2008.

[30] J. Xue, W. Liang, X. Liu, Q. Shen, and B. Xu, "Crystallization behavior and formation mechanism of dendrite Cu_2O crystals," *CrystEngComm*, vol. 14, no. 23, pp. 8017–8022, 2012.

[31] M. R. Hoffmann, S. T. Martin, W. Choi, and D. W. Bahnemann, "Environmental applications of semiconductor photocatalysis," *Chemical Reviews*, vol. 95, no. 1, pp. 69–96, 1995.

[32] N. Jain, A. Bhargava, and J. Panwar, "Enhanced photocatalytic degradation of methylene blue using biologically synthesized 'protein-capped' ZnO nanoparticles," *Chemical Engineering Journal*, vol. 243, pp. 549–555, 2014.

[33] S.-M. Lam, J.-C. Sin, A. Z. Abdullah, and A. R. Mohamed, "Degradation of wastewaters containing organic dyes photocatalysed by zinc oxide: a review," *Desalination and Water Treatment*, vol. 41, no. 1–3, pp. 131–169, 2012.

[34] C.-J. Lin, Y.-T. Lu, C.-H. Hsieh, and S.-H. Chien, "Surface modification of highly ordered TiO_2 nanotube arrays for efficient photoelectrocatalytic water splitting," *Applied Physics Letters*, vol. 94, no. 11, Article ID 113102, 2009.

[35] S.-Y. Pung, W.-P. Lee, and A. Aziz, "Kinetic study of organic dye degradation using ZnO particles with different morphologies as a photocatalyst," *International Journal of Inorganic Chemistry*, vol. 2012, Article ID 608183, 9 pages, 2012.

[36] X. Jia, M. Tian, Y. Liu, X. Wu, and H. Song, "In situ precipitation preparation of ZnO hollow spheres and their photocatalysis and gas-sensing properties," *Applied Physics A*, vol. 119, no. 3, pp. 1179–1185, 2015.

[37] S. Licht, B. Wang, S. Mukerji, T. Soga, M. Umeno, and H. Tributsch, "Efficient solar water splitting, exemplified by RuO_2-catalyzed AlGaAs/Si photoelectrolysis," *The Journal of Physical Chemistry B*, vol. 104, no. 38, pp. 8920–8924, 2000.

[38] S. Licht, B. Wang, S. Mukerji, T. Soga, M. Umeno, and H. Tributsch, "Over 18% solar energy conversion to generation of hydrogen fuel; theory and experiment for efficient solar water splitting," *International Journal of Hydrogen Energy*, vol. 26, no. 7, pp. 653–659, 2001.

[39] C. W. Lai and S. Sreekantan, "Photoelectrochemical properties of TiO_2 nanotube arrays: effect of electrolyte pH and annealing temperature," *Journal of Experimental Nanoscience*, vol. 9, no. 3, pp. 230–239, 2014.

[40] K.-S. Ahn, S. Lee, A. C. Dillon, C. E. Tracy, and R. Pitts, "The effect of thermal annealing on photoelectrochemical responses of WO_3 thin films," *Journal of Applied Physics*, vol. 101, no. 9, Article ID 093524, 2007.